# Effects of ion and nanosecond-pulsed laser co-irradiation on the surface nanostructure of Au thin films on SiO2 glass substrates

Ruixuan Yu, Tamaki Shibayama, Xuan Meng, Shinya Takayanagi, Shigeo Yatsu, Junya Ishioka, and Seiichi Watanabe

Citation: Journal of Applied Physics **115**, 143104 (2014); doi: 10.1063/1.4871016
View online: http://dx.doi.org/10.1063/1.4871016
View Table of Contents: http://scitation.aip.org/content/aip/journal/jap/115/14?ver=pdfcov
Published by the AIP Publishing

# Effects of ion and nanosecond-pulsed laser co-irradiation on the surface nanostructure of Au thin films on $SiO_2$ glass substrates

Ruixuan Yu,[1] Tamaki Shibayama,[2,a)] Xuan Meng,[1] Shinya Takayanagi,[1] Shigeo Yatsu,[2] Junya Ishioka,[2] and Seiichi Watanabe[2]
[1]*Graduate School of Engineering, Hokkaido University, Sapporo, Hokkaido 060-8628, Japan*
[2]*Center for Advanced Research of Energy and Materials Science, Faculty of Engineering, Hokkaido University, Sapporo, Hokkaido 060-8628, Japan*

(Received 23 December 2013; accepted 31 March 2014; published online 9 April 2014)

Ion irradiation and short-pulsed laser irradiation can be used to form nanostructures on the surfaces of substrates. This work investigates the synergistic effects of ion and nanosecond-pulsed laser co-irradiation on surface nanostructuring of Au thin films deposited under vacuum on $SiO_2$ glass substrates. Gold nanoparticles are randomly formed on the surface of the substrate after nanosecond-pulsed laser irradiation under vacuum at a wavelength of 532 nm with a repetition rate of 10 Hz and laser energy density of 0.124 kJ/m$^2$. Gold nanoparticles are also randomly formed on the substrate after 100-keV $Ar^+$ ion irradiation at doses of up to $3.8 \times 10^{15}$ ions/cm$^2$, and nearly all of these nanoparticles are fully embedded in the substrate. With increasing ion irradiation dose (number of incident laser pulses), the mean diameter of the Au nanoparticles decreases (increases). However, Au nanoparticles are only formed in a periodic surface arrangement after co-irradiation with 6000 laser pulses and $3.8 \times 10^{15}$ ions/cm$^2$. The periodic distance is ~540 nm, which is close to the wavelength of the nanosecond-pulsed laser, and the mean diameter of the Au nanoparticles remains at ~20 nm with a relatively narrow distribution. The photoabsorption peaks of the ion- or nanosecond-pulsed laser-irradiated samples clearly correspond to the mean diameter of Au nanoparticles. Conversely, the photoabsorption peaks for the co-irradiated samples do not depend on the mean nanoparticle diameter. This lack of dependence is likely caused by the periodic nanostructure formed on the surface by the synergistic effects of co-irradiation. © *2014 AIP Publishing LLC*. [http://dx.doi.org/10.1063/1.4871016]

## I. INTRODUCTION

Noble metal nanoparticle/dielectric systems containing metals such as Au can exhibit nonlinear optical properties such as localized surface plasmon resonance (LSPR).[1] The LSPR frequency of a nanoparticle/dielectric system is correlated with the size and shape of the nanoparticles,[2,3] interparticle distance,[4] and the dielectric environment surrounding them. By tuning the LSPR frequency using these factors, metallic nanoparticle/dielectric systems can be devised for applications such as biosensors,[5–11] plasmonic waveguides,[12] and photocatalysts.[13]

Metallic nanostructures can be prepared on the surface of metallic thin films deposited on dielectric or semiconductor substrates via irradiation of the surface with a quantum beam such as an ion beam,[14–23] nanosecond-pulsed laser,[24,25] or electron beam.[26] Surface nanostructures are formed by dewetting caused by irradiation with a quantum beam.[14–26] Under ion irradiation, metal nanoparticles that form on the surface through the dewetting process become embedded in $SiO_2$ glass[21,23] and $Al_2O_3$[22] substrates because the viscosity of the substrate changes and it undergoes plastic flow during ion irradiation.[16,19] Laser-induced periodic surface structures (LIPSS) can be obtained via nanosecond-pulsed laser irradiation. LIPSS formation strongly depends on the laser wavelength, electric field vector, and polarization direction.[27–30] For example, Kiesow *et al.*[28] generated periodic Au nanostructures in Au nanoparticle-containing polymer films on glass substrates by short-pulsed laser irradiation.

Quantum beam co-irradiation studies using a heavy ion beam and nanosecond-pulsed laser beam[32–37] or an electron beam and nanosecond-pulsed laser beam[38,39] have also been reported. Intense heavy ion beams and high-energy laser systems are used to study the beam-plasma interactions of matter with high energy density in plasma physics and fusion research.[37] Kishimoto *et al.*[32–36] have studied metal nanoparticle formation induced by heavy ion and nanosecond-pulsed laser co-irradiation. Studies on the modification of material properties using heavy ion and nanosecond-pulsed laser co-irradiation methods have focused on radiation damage annihilation and the aggregation of implanted atoms. Little research on the surface nanostructuring of metallic thin film/dielectric substrates using rare gas ion beam and nanosecond-pulsed laser co-irradiation has been reported.

Herein, we examine $Ar^+$ ion irradiation-induced formation of nanoparticles embedded in a substrate and laser irradiation-induced periodic surface structuring. Recently, we synthesized noble metal nanoparticles with a narrow size distribution embedded in $SiO_2$ glass substrates[21,23] and $Al_2O_3$ single-crystal substrates[22] via $Ar^+$ ion irradiation. We also synthesized Au nanoparticles that formed periodic arrays on $SiO_2$ glass substrates through nanosecond-pulsed laser irradiation.[31] LIPSS formation strongly depended on the laser energy density, number of laser pulses, and electric field vector of the incident laser.[27–31] Considering the results

a)Electronic mail: shiba@qe.eng.hokudai.ac.jp.

 

of the above studies, we decided to investigate the effects of $Ar^+$ ion beam and nanosecond-pulsed laser co-irradiation on the formation of $Au/SiO_2$ nanostructures. We anticipate that co-irradiation will accelerate the formation of periodic structures because of our previous results showing that the LSPR frequency depended on the morphology (size, embedded depth, and interparticle distance) of the formed nanostructures.[21–23,31] Microstructural analyses of the samples are performed using scanning electron microscopy (SEM) and transmission electron microscopy (TEM). The optical absorbance of the samples is also measured, with emphasis on the correlation between their optical properties and nanostructures.

## II. EXPERIMENTAL PROCEDURE

$SiO_2$ glass substrates with a diameter of 10 mm and mirror finish on both sides (Shin-Etsu Chemical Co., Ltd., Tokyo, Japan, O-H density: 80–100 ppm) were used. The substrates were 1.0 mm thick with a visible light transmittance of 90%. A thin Au layer (Au source purity of 99.9%) was deposited on each $SiO_2$ glass substrate at room temperature by electrically heating the Au source using a custom-built vacuum evaporator operating at a pressure of $1.1 \times 10^{-2}$ Pa.

The irradiation experiments were performed in a vacuum chamber maintained at $4.0 \times 10^{-4}$ Pa. The surface of the Au thin film on the $SiO_2$ glass substrate was irradiated with a linearly polarized Nd-YAG nanosecond-pulsed laser (Inlite II; Continuum Co., Ltd., CA, USA) in a perpendicular orientation. The nanosecond-pulsed laser operated at a wavelength of 532 nm with a nominal pulse duration of 5–7 ns. The average laser energy density was 0.124 J/cm$^2$, and the repetition rate was 10 Hz. The laser beam was introduced into the vacuum chamber through a quartz glass window (ES grade; Tosoh Co., Ltd., Tokyo, Japan) with 90% transmittance of 532-nm light. The electric field vector (***E***) of the laser was parallel to the floor surface. To examine the dependence of nanostructure development on the number of laser pulses, samples were irradiated with 3000, 6000, and 7500 pulses (referred to as L-300, L-600, and L-750, respectively) with irradiation times of 300, 600, and 750 s, respectively.

To examine the dependence of nanostructure development on the ion fluence of the ion irradiation, samples were irradiated at ambient temperature with 100-keV $Ar^+$ ions with fluences of 1.9, 3.8, and $4.7 \times 10^{15}$ Ar ions/cm$^2$ (referred to as I-300, I-600, and I-750, respectively). To ensure a uniform ion irradiation dose, the $Ar^+$ ion beam was scanned over the substrate, and the ion current was maintained at approximately 1.0 $\mu$A/cm$^2$ ($6.25 \times 10^{12}$ ions/cm$^2$s). Suitable accelerating energies for the $Ar^+$ ions were selected based on the thickness of the Au layer on each $SiO_2$ glass substrate estimated using the SRIM 2011 code.[40] $Ar^+$ ion beam irradiation of the samples was performed using the 400-kV ion accelerator at the High Voltage Electron Microscope Laboratory located at Hokkaido University.[41] $Ar^+$ ions were irradiated onto the surface of the Au thin film on each $SiO_2$ glass substrate at an angle of 40°.

$Ar^+$ ion beam and nanosecond-pulsed laser co-irradiation were performed using the corresponding $Ar^+$ ion fluences (I-300, I-600, and I-750) with nanosecond-pulsed laser pulses of L-300, L-600, and L-750, respectively, and are referred to as co-300, co-600, and co-750, respectively. The irradiation conditions are summarized in Table I.

After irradiation, photoabsorbance measurements were performed with a spectrophotometer (JASCO, V-630, Tokyo, Japan) using a circular slit with a diameter of 1.0 mm to confine the irradiated region. The surface morphology of the samples was observed by SEM (JEOL, JSM-7001FA, Tokyo, Japan), and cross-sectional microstructural analyses were performed via TEM (JEOL, JEM-2010F). Cross-sectional TEM (X-TEM) samples were prepared using focused-ion beam equipment (FIB; JEOL, JEM-9320). The elemental concentration of the samples was determined using an energy-dispersive spectrometer (EDS: Noran, Thermo Fisher Scientific, MA, USA) in conjunction with the TEM.

## III. RESULTS

Figure 1 shows SEM images of the surface morphology (Fig. 1(a)) and X-TEM images (Fig. 1(b)) of the deposited Au thin films on the $SiO_2$ glass substrates. The X-TEM images reveal that the Au thin films are approximately 10–15 nm thick (the designated thickness is 10 nm). It should be noted that a carbon layer (hereafter referred to as the C layer) was deposited on the surface of each X-TEM sample (Fig. 1(b)) to protect it during FIB sample preparation.

Figures 2(a)–2(c) show SEM images of the surface morphology after $Ar^+$ ion irradiation with different fluences (I-300, I-600, and I-750, respectively), while Figs. 2(d)–2(f) present SEM images of the surface morphology after nanosecond-pulsed laser irradiation with different pulses (L-300, L-600, and L-750, respectively). SEM images of the surface morphology after $Ar^+$ ion and nanosecond-pulsed laser co-irradiation with different fluences and pulses (co-300, co-600, and co-750) are depicted in Figs. 2(g)–2(i), respectively. The Au nanoparticles can be studied in detail by analyzing these SEM images. Figs. 2(h) and 2(j) reveal that a periodic structure only forms on the surface of the $SiO_2$ glass substrate after co-irradiation for 600 s (co-600). The periodic structure has an average width of approximately 275 nm, and the average distance between periodic structures is approximately 540 nm. Because the periodic

TABLE I. Irradiation conditions used to prepare the samples.

| Sample | Irradiation mode | Ion dose/ions/cm$^2$ | Number of laser pulses | Irradiation time/s |
|---|---|---|---|---|
| I-300 | Ion irradiation | $1.9 \times 10^{15}$ | … | 300 |
| I-600 | Ion irradiation | $3.8 \times 10^{15}$ | … | 600 |
| I-750 | Ion irradiation | $4.7 \times 10^{15}$ | … | 750 |
| L-300 | Laser irradiation | … | 3000 | 300 |
| L-600 | Laser irradiation | … | 6000 | 600 |
| L-750 | Laser irradiation | … | 7500 | 750 |
| co-300 | Co-irradiation | $1.9 \times 10^{15}$ | 3000 | 300 |
| co-600 | Co-irradiation | $3.8 \times 10^{15}$ | 6000 | 600 |
| co-750 | Co-irradiation | $4.7 \times 10^{15}$ | 7500 | 750 |

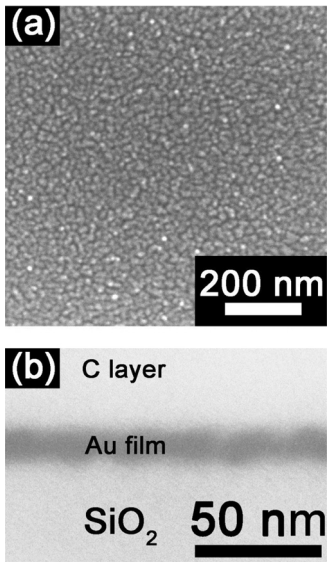


FIG. 1. (a) SEM and (b) X-TEM images of a 10-nm-thick Au film deposited on an $SiO_2$ glass substrate.

interval is approximately equivalent to the wavelength of the incident nanosecond-pulsed laser used in this study, the periodic structure is thought to be a LIPSS.

Figures 3(a)–3(i) show histograms of the diameters of the Au nanoparticles on the substrates after irradiation. Because the distributions of the diameters of the Au nanoparticles appear to be asymmetric, the average diameter was statistically determined using a fitting method called the Gumbel distribution. The mode value ($\mu$) and distribution scale ($\theta$) were obtained from the results of the fitting, with mean values, $\langle D \rangle$, determined as follows:

$$\langle D \rangle = \mu + \gamma\theta, \tag{1}$$

where $\gamma$ is Euler's constant ($\sim$0.5772). Because Au nanoparticles with diameters of several tens of nanometers can exhibit LSPR,[2] it is important to determine their diameters. Each mean diameter value, $\langle D \rangle$, determined from the SEM results presented in Fig. 2 is shown in the corresponding histogram in Fig. 3.

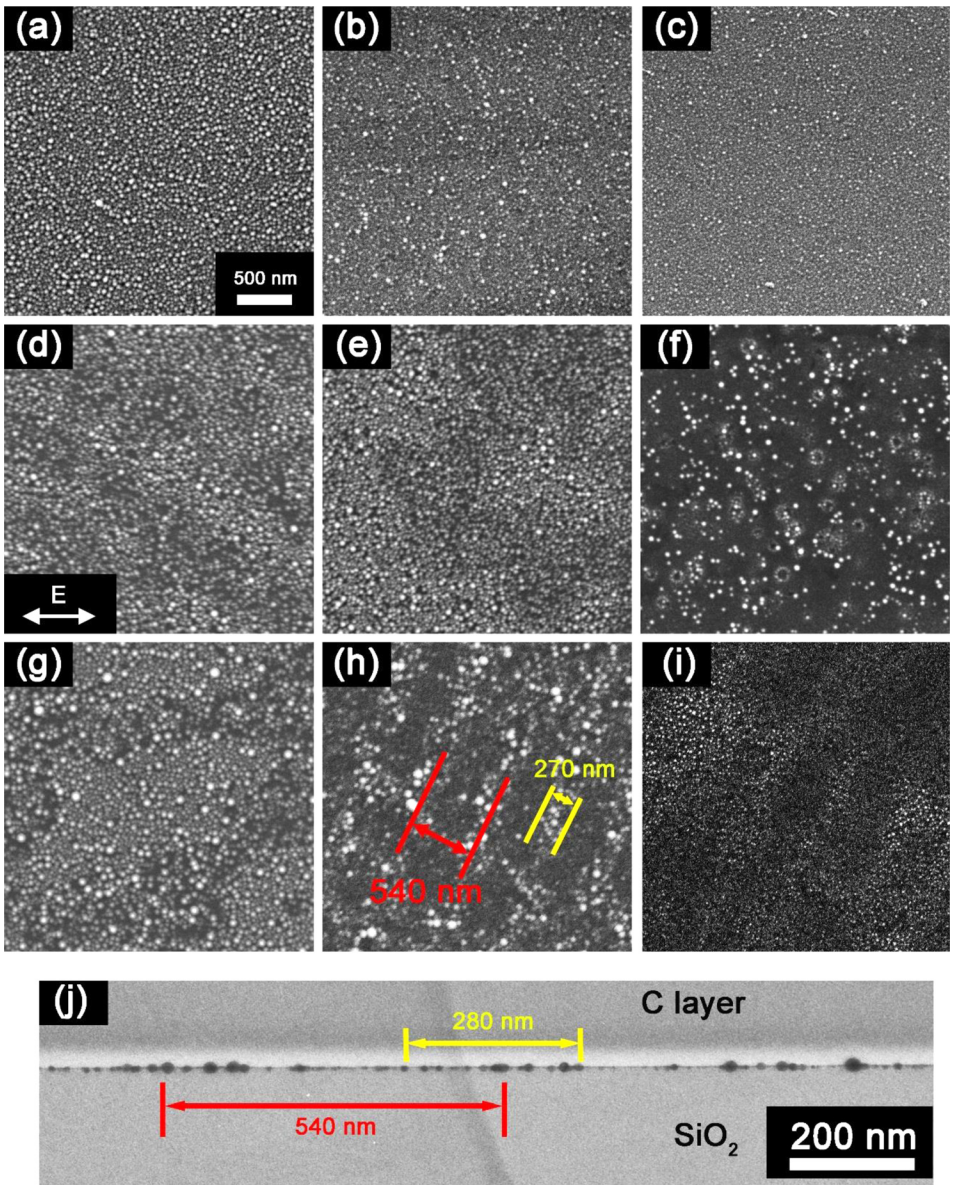


FIG. 2. SEM images of the $Au/SiO_2$ system after ion irradiation for (a) 300, (b) 600, and (c) 750 s; after laser irradiation for (d) 300, (e) 600, and (f) 750 s; and after ion and laser co-irradiation for (g) 300, (h) 600, and (i) 750 s, respectively. (j) X-TEM image of the periodic nanostructures in sample co-600. The ***E*** vector indicates the electric field vector of the laser light on the surface during laser irradiation.

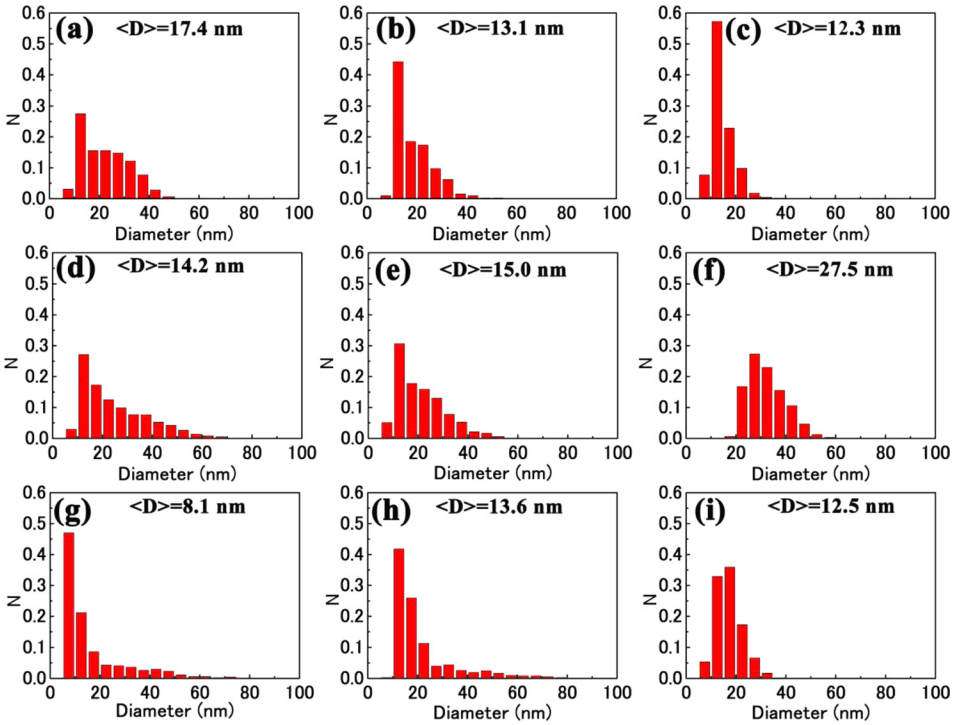


FIG. 3. (a)–(i) Distribution of nanoparticle diameters obtained from the corresponding SEM image in Figs. 2(a)–2(i). N is the proportion of Au nanoparticles.

Nanoparticles form on the surface of the sample after each $Ar^+$ ion irradiation period. Figures 3(a)–3(c) show that the mean diameter of the nanoparticles decreases as the irradiation time increases from 300 to 750 s. Nanoparticles also form on the surface of the substrate after each nanosecond-pulsed laser irradiation period. The mean diameter of these nanoparticles increases as the irradiation time increases from 300 to 750 s (Figs. 3(d)–3(f)). However, LIPSS are not formed after nanosecond-pulsed laser irradiation only. When the samples are co-irradiated (Figs. 3(g) and 3(h)), the mean diameter of the nanoparticles increases with irradiation time from 300 to 600 s, and then decreases as the irradiation time increases further to 750 s.

Next, the detailed microstructure of the nanoparticles formed on the surfaces of the samples after irradiation was examined by X-TEM observation; the resulting images are presented in Fig. 4. Figures 4(a)–4(c) reveal that the Au thin film disappears between the nanoparticles after $Ar^+$ ion irradiation for 300 s or more, and the nanoparticles are almost completely embedded in the $SiO_2$ glass substrate after $Ar^+$ ion irradiation for 600 s. Conversely, the Au thin film remains between the nanoparticles on the surfaces of the $SiO_2$ glass substrates after all co-irradiation times (Figs. 4(d)–4(f)). After co-irradiation for 600 s, the nanoparticles are only embedded halfway into the $SiO_2$ glass substrate.

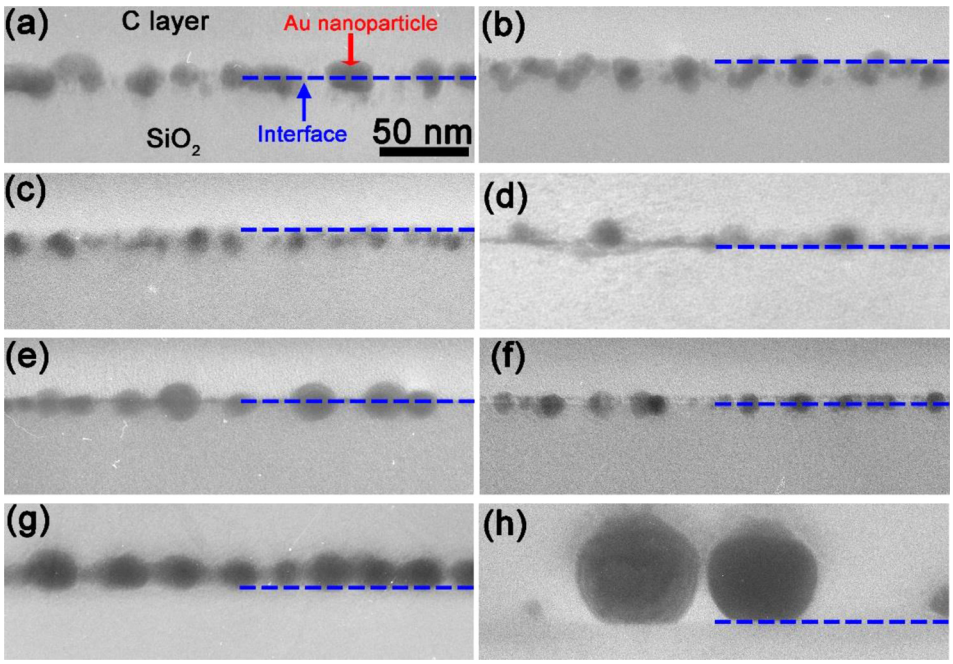


FIG. 4. X-TEM images of samples (a) I-300, (b) I-600, (c) I-750, (d) co-300, (e) co-600, (f) co-750, (g) L-600, and (h) L-750. Blue dashed lines indicate the interface between each Au layer and substrate.

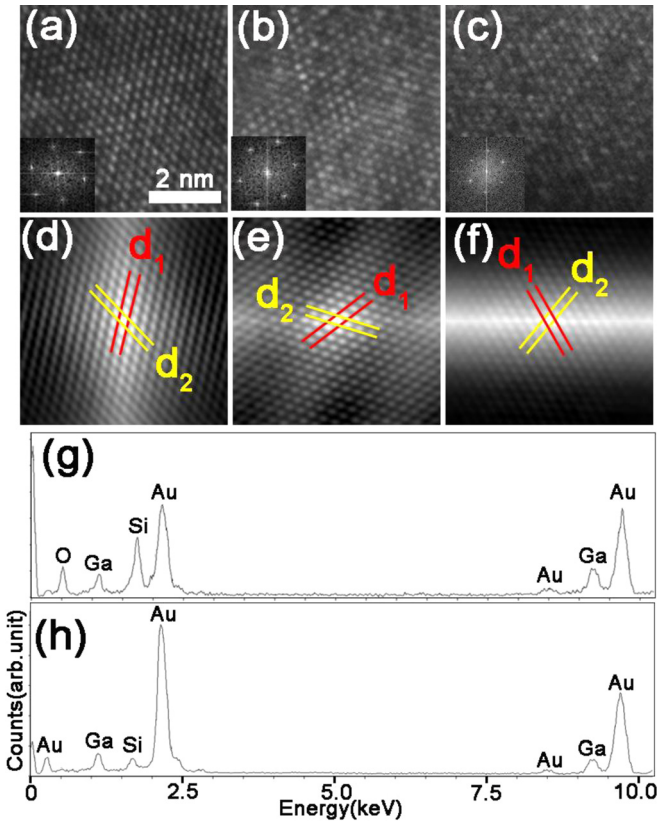


FIG. 5. High-resolution X-TEM images of samples (a) I-300, (b) co-300, and (c) L-750; the corresponding FFT patterns for these samples are shown in the insets. (d), (e) and (f) Two-dimensional ACF images obtained for (a)–(c), respectively. EDS spectra corresponding to (g) Fig. 5(a) and (h) Fig. 5(c), respectively.

Figures 5(a)–5(c) present high-resolution X-TEM images and the corresponding fast Fourier transform (FFT) patterns for I-300, co-300, and L-750, respectively. Analysis of the high-resolution X-TEM images indicates that the nanoparticles formed are single crystals. Figures 5(g) and 5(h) depict EDS data measured for the samples shown in Figs. 5(a) and 5(c), respectively; the quantitative results of the EDS elemental analyses are listed in Table II. The Si concentration of I-300 is higher than that of L-750. Figures 5(d)–5(f) depict the autocorrelation function (ACF) images obtained from the FFTs in Figs. 5(a)–5(c), respectively. The lattice spacings of the nanoparticles obtained from the ACF images are listed in Table III. In the high-resolution images of I-300 and co-300, the $d_1$ and $d_2$ spacings are consistent with the (211) and (220) lattice spacings of a meta-equilibrium Au-Si alloy ($Au_5Si$: $d_{211} = 0.275$ nm, $d_{220} = 0.238$ nm), respectively.[42] It is therefore likely that the nanoparticles in I-300 and co-300 consist of this meta-equilibrium alloy of Au-Si. Conversely, in the high-resolution image of L-750, the $d_1$ and $d_2$ spacings are consistent with the (111) lattice spacing of an Au single crystal ($d_{111} = 0.235$ nm).[43] This suggests that the nanoparticles that form on the substrate surface after nanosecond-pulsed laser irradiation have Au crystalline structure (see S2 in the supplementary information[46]). It should be noted that the Ga peaks in the EDS are caused by preparation of the samples for X-TEM analysis using the FIB system. Hereafter, all of the nanoparticles are referred to as Au nanoparticles regardless of composition.

TABLE II. Atomic concentrations of Au, Si, and O (%) obtained from the EDS data presented in Figs. 5(a) and 5(c).

| Sample | Au atomic concentration | Si atomic concentration | O atomic concentration |
|---|---|---|---|
| I-300 | 46.96 | 21.50 | 31.53 |
| L-750 | 77.77 | 3.24 | 18.98 |

TABLE III. Lattice spacings obtained from the high-resolution X-TEM images in Fig. 5.

| Sample | $d_1$ (nm) | $d_2$ (nm) |
|---|---|---|
| I-300 | 0.276 | 0.235 |
| co-300 | 0.277 | 0.238 |
| L-750 | 0.236 | 0.235 |

Next, to clarify the optical properties of the nanoparticles dispersed on the $SiO_2$ glass substrates, photoabsorbance spectra of irradiated samples were obtained. Figures 6(a)–6(c) show photoabsorbance spectra of the regions containing Au nanoparticles after ion irradiation, laser irradiation, and co-irradiation, respectively. Each spectrum has a clear peak corresponding to a LSPR-enhanced absorption. The LSPR peak wavelengths are summarized in Fig. 6(d). The position of the LSPR peak wavelength is directly related to the irradiation time and method.

The relationship between the LSPR peak wavelength (Fig. 6(d)) and mean nanoparticle diameter (Fig. 3) was then investigated. For the ion-irradiated samples, an increased irradiation time leads to a blue shift of LSPR peak wavelength. In contrast, the LSPR peak wavelength of the nanosecond-pulsed laser irradiated samples shifts to longer wavelength as the irradiation time increases. Therefore, the changes of the LSPR peak wavelengths match those of the mean diameters of the nanoparticles for these samples. Conversely, the mean diameter of the Au nanoparticles of co-600 is larger than those of co-300, and the Au nanoparticles of co-600 are embedded approximately halfway into the $SiO_2$ glass substrate. However, the LSPR peak for co-600 is blue shifted from that of co-300.

## IV. DISCUSSION

The Heywood diameter (area equivalent to the diameter of a circle) of the as-evaporated Au thin film on a $SiO_2$ glass substrate was obtained from a X-TEM image. The as-evaporated Au thin film is composed of grains with sizes in the range of 5–40 nm. The average Heywood diameter of the grains is approximately 14.6 nm (see S3 in the supplementary information[46]), which is almost the same as those of Au nanoparticles on a $SiO_2$ glass substrate after ion irradiation for 300 s (Fig. 3(a); I-300) and laser irradiation for 300 s (Fig. 3(d); L-300). However, the size distributions of grains and nanoparticles in these samples are quite different from each other. The average size of nanoparticles after ion and

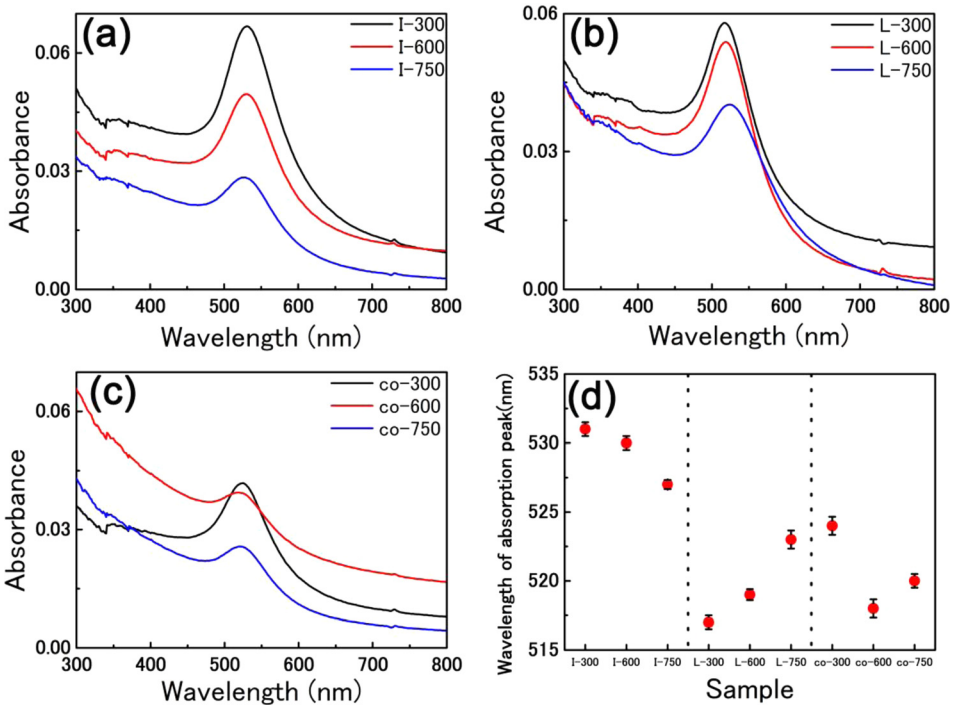


FIG. 6. (a) Photoabsorbance spectra of I-300, I-600, and I-750. (b) Photoabsorbance spectra of L-300, L-600, and L-750. (c) Photoabsorbance spectra of co-300, co-600, and co-750. (d) Comparison of the wavelengths of the absorption peaks of the samples.

laser co-irradiation for 300 s (Fig. 3(g); co-300) is much smaller than those of I-300, L-300 and as-evaporated Au grains. Therefore, ion and laser co-irradiation strongly affected the formation and size distribution of nanoparticles.

In the case of $Ar^+$ ion irradiation, the $Ar^+$ ions impart kinetic energy to the Au thin films, inducing multiple collisions events and the diffusion of Au atoms. Bombardment with ions that are sufficiently higher than the threshold energy will also cause thermal energy transfer to the target because of inelastic collision during irradiation. This is a general phenomenon that is called ion beam heating during irradiation. Nanosecond-pulsed laser irradiation will also heat the samples. As a result, the Au thin films take on the properties of the liquid state, and dewetting of the films occurs.[14,15,17–23] At the beginning of dewetting, holes grow on the surface of the thin film, and continues to expand. Generally, grain boundaries play an important role in hole formation. If the holes grow large enough, they impinge to form islands; the size of which are determined by the surface energies.[48] Some of the Au atoms are also removed by sputtering during $Ar^+$ ion irradiation, causing the Au film thickness to decrease as the irradiation dose increases.[20]

The $Ar^+$ ion collision events (the stopping range in the 10-nm-thick Au films deposited on the $SiO_2$ glass substrate) was simulated using the SRIM 2011 code.[40] Most of the 100-keV $Ar^+$ ions should transmit through the Au thin film and stop in the substrate. Thus, the $Ar^+$ ions will also induce radiation effects in the $SiO_2$ glass substrate. $Ar^+$ ion irradiation in a direction perpendicular to the surface of a 10-nm-thick Au film on the $SiO_2$ glass substrate side is estimated to result in an Au atom sputtering rate of approximately 7.2 atoms/ion. This sputtering rate increases to 14.5 atoms/ion for ion irradiation 40° to the surface of Au thin films on $SiO_2$ glass substrates.

During nanosecond-pulsed laser irradiation, the Au thin films absorb the photon energy of the laser light, the Au atoms are excited by the electromagnetic field, and the temperature of the Au thin films reaches melting point when the incident laser power density is sufficiently high.[44] For example, during heating, grain boundaries will relax and rearrange, so recrystallization (rearrangement) will occur provided there is sufficient heating temperature and time. In this study, the heating temperature is sufficiently high, but there is not enough time for recrystallization, so the grain boundaries only retract to reduce the surface and grain boundary energy during irradiation and initiate dewetting. As a result, Au nanoparticles are formed on the surface of the Au thin films on $SiO_2$ glass substrates by laser-induced dewetting processes.[31] It should be noted that because the $SiO_2$ glass substrate transmits 90% of 532-nm light, the interaction of the nanosecond-pulsed laser with the substrate is negligible.

Generally, LIPSS are formed as a result of the interference between the incident laser light and the scattered waves on the surface,[27–30] which enhances the interactions between the laser light and material. For example, the temperature of the Au thin films rapidly increases and decreases during nanosecond-pulsed laser irradiation, causing the Au thin films to alternately melt and solidify. After the initiation of nanosecond-pulsed laser irradiation, the Au thin films fragment because of the surface tension created during the above process. These fragments then repeatedly melt and solidify, ultimately forming Au nanoparticles on the $SiO_2$ glass substrate via the above-mentioned dewetting process. Conversely, in regions where there is little interference, the Au thin films do not absorb sufficient energy to form Au nanoparticles. In this case, the nanoparticles formed by nanosecond-pulsed laser irradiation are much smaller than those obtained in our previous study.[31] The scattering angle between the incident laser light and nanoparticles strongly depends on the size of the nanoparticles.[45] When the ***E***

vector of the incident laser light is parallel to the floor surface, the intensity of the wide-angle scattered light of the particles is weak and can be determined using Mie scattering theory.[45] Therefore, the effect of the interference between the incident laser light and scattered laser light on the nanoparticles is not sufficient for LIPSS formation.

The diameter of the Au nanoparticles decreases as the $Ar^+$ ion irradiation time increases from 300 to 750 s because of $Ar^+$ ion sputtering of the nanoparticles. Conversely, prolonging the nanosecond-pulsed laser irradiation time from 300 to 750 s increases the diameter of the Au nanoparticles because of the aggregation of smaller Au nanoparticles after remelting. Therefore, during $Ar^+$ ion and nanosecond-pulsed laser co-irradiation, these two processes compete, causing an initial increase and subsequent decrease of nanoparticle diameter with extending irradiation time.

Notably, after laser irradiation for 750 s, the Au nanoparticles are randomly distributed on the surface of the $SiO_2$ glass substrate. The formation of LIPSS strongly depends on the energy distribution profile (see S1 in the supplementary material[46]). Because nanosecond-pulsed laser irradiation occurred through a quartz glass window, the energy distribution profile of the laser beam is not homogeneous. Generally, LIPSS can be formed only at the appropriate energy density; we previously revealed the necessary conditions for LIPSS formation in air with respect to the repletion rate and energy density of the nanosecond-pulsed laser used in this study.[31,46] The thickness of the Au thin film deposited on the $SiO_2$ glass substrate also influences the formation of LIPSS via nanosecond-pulsed laser irradiation. However, a periodic structure is formed only after co-irradiation for 600 s. This suggests that during co-irradiation, the $Ar^+$ ion irradiation-induced dewetting of the Au thin films accelerates the formation of a periodic structure. Additionally, because $Ar^+$ ion irradiation at 40° to the surface increases sputtering, the periodic structure disappears for co-irradiation times greater than 600 s.

Numerous defects, such as vacancies and interstitial atoms, are generated in the solid amorphous $SiO_2$ glass substrate under $Ar^+$ ion irradiation. $Ar^+$ ion irradiation also causes the solid substrate to become viscous and flow in the ion irradiation region.[16,19] The nanoparticles thus become embedded in the viscous $SiO_2$ glass substrate as a result of the ion-induced burrowing effect.[16,19] The defects in the amorphous $SiO_2$ are self-trapped holes with optical absorption bands near 2.2 eV.[36,47] Therefore, the incident 532-nm nanosecond-pulsed laser and $SiO_2$ glass substrate will interact, which is assumed to influence the depth at which the Au nanoparticles are embedded during co-irradiation. However, there is not yet a comprehensive explanation for how this interaction influences the embedded depth of the Au nanoparticles; clarification of this mechanism is a topic for future investigation. It should also be noted that some Si atoms are injected into the Au thin film from the $SiO_2$ glass substrate under $Ar^+$ ion irradiation. These Si atoms mix with the Au atoms, resulting in the formation of an Au-Si alloy on the surface of the nanoparticles.

It has been reported that for Au nanoparticles in a dielectric solution, a decrease in the mean diameter of the nanoparticles leads to a blue shift of LSPR, while an increase in the mean diameter of the nanoparticles leads to a red shift of the LSPR peak.[2] In this work, the mean diameters of the nanoparticles in L-300, L-600, and L-750 are larger than that of I-750, but the wavelengths of the LSPR peaks for these samples are blue shifted compared with that of I-750. Lance Kelly *et al.*[3] correlated the LSPR peak of nanoparticles with the weighted average dielectric constant for the contact area of each dielectric. In our study, photoabsorbance was measured in air (dielectric constant of 1.0) and through the $SiO_2$ glass substrate (dielectric constant of 3.9). The weighted average of the dielectric constant of the Au nanoparticles embedded in the $SiO_2$ glass substrate is higher than that of the Au nanoparticles on the surface of the $SiO_2$ glass substrate, so the LSPR peak is red shifted.

Rechberger *et al.*[4] investigated the effects of the polarization direction of the incident light and interparticle distance on LSPR peak wavelength. They found that when the polarization direction was parallel to the two-dimensional (2D) particle arrangement, a decrease in interparticle distance led to a red shift of the LSPR peak. However, when the polarization was orthogonal to the 2D particle arrangement, a decrease in the interparticle distance led to a blue shift of the LSPR peak. This behavior was explained by a simple weakening/enhancing of the restoring forces for the plasma electrons caused by the charge distribution of the neighboring particles.

Because the spectrophotometer used in the present study does not enable precise control of the polarization of the incident light, the relationship between the visible absorption spectrum and polarization of the incident light cannot be determined. However, the mean diameter of the Au nanoparticles in co-600 is larger than that of co-300, but the LSPR of co-600 with a periodic structure of nanoparticles on the $SiO_2$ substrate is blue shifted from that of co-300 with no periodic structure on the surface. This blue shift may thus be related to the different distribution of Au nanoparticles in these two samples and is evidence for the formation of LIPSS.

## V. CONCLUSIONS

The characteristics of periodic structures generated via nanosecond-pulsed laser irradiation combined with uniformly dispersed nanoparticles formed by $Ar^+$ ion irradiation were evaluated with the goal of obtaining materials with new optical properties induced by the periodic arrangement of nanoparticles on the surface. Therefore, the fabrication of Au nanoparticles on Au thin films deposited on $SiO_2$ glass substrates via $Ar^+$ ion irradiation alone, nanosecond-pulsed laser irradiation alone, and co-irradiation with $Ar^+$ ions and a nanosecond-pulsed laser was investigated. A periodic structure (LIPSS) formed on the surface of the $SiO_2$ glass substrate only after 600 s of $Ar^+$ ion and nanosecond-pulsed laser co-irradiation. When only $Ar^+$ ion irradiation or nanosecond-pulsed laser irradiation was used, the LSPR shifts are in good agreement with the changes in the mean diameter of the Au nanoparticles. However, LIPSS formation as a result of $Ar^+$ ion and nanosecond-pulsed laser co-irradiation leads to unexpected LSPR shifts, possibly because of the effects of the charge distribution around the Au nanoparticles resulting from the relative differences in

the distances between the Au nanoparticles formed by LIPSS. Based on these results, this co-irradiation technique is expected to be useful for the development of advanced optical devices using LIPSS.

## ACKNOWLEDGMENTS

This study was conducted at Hokkaido University and was supported by the "Nanotechnology Platform" Program of the Ministry of Education, Culture, Sports, Science and Technology (MEXT), Japan (Grant No. HNPA 13_031). The authors thank Mr. K. Ohkubo, Dr. Z. Yang, Dr. Y. Yoshida, and Mrs. Yamamoto for their technical assistance and helpful discussion.

[1]E. Hutter and J. H. Fendler, Adv. Mater. **16**(19), 1685–1706 (2004).
[2]S. Link and M. A. El-Sayed, J. Phys. Chem. B **103**, 4212–4217 (1999).
[3]K. Lance Kelly, E. Coronado, L. L. Zhao, and G. C. Schatz, J. Phys. Chem. B **107**, 668–677 (2003).
[4]W. Rechberger, A. Hohenau, A. Leitner, J. R. Krenn, B. Lamprecht, and F. R. Aussenegg, Opt. Commun. **220**, 137–141 (2003).
[5]N. Nath and A. Chilkoti, Anal. Chem. **74**, 504–509 (2002).
[6]L. Olofsson, T. Rindzevicius, I. Pfeiffer, M. Kall, and F. Hook, Langmuir **19**, 10414–10419 (2003).
[7]A. J. Haes and R. P. Van Duyne, Anal. Bioanal. Chem. **379**, 920–930 (2004).
[8]T.-J. Lin, K.-T. Huang, and C.-Y. Liu, Biosens. Bioelectron. **22**, 513–518 (2006).
[9]T.-J. Lin and M.-F. Chung, Biosens. Bioelectron. **24**, 1213–1218 (2009).
[10]A. Prabhakar and S. Mukherji, Lab Chip **10**, 3422–3425 (2010).
[11]M. Prabha Singh and G. F. Strouse, J. Am. Chem. Soc. **132**, 9383–9391 (2010).
[12]K.-Y. Jung, F. L. Teixeira, and R. M. Reano, J. Lightwave Technol. **25**(9), 2757–2765 (2007).
[13]S. Sato, T. Arai, T. Morikawa, K. Uemura, T. M. Suzuki, H. Tanaka, and T. Kajino, J. Am. Chem. Soc. **133**, 15240–15243 (2011).
[14]X. Hu, D. G. Cahill, and R. S. Averback, Appl. Phys. Lett. **76**, 3215–3217 (2000).
[15]X. Hu, D. G. Cahill, and R. S. Averback, J. Appl. Phys. **89**, 7777–7783 (2001).
[16]X. Hu, D. G. Cahill, and R. S. Averback, J. Appl. Phys. **92**, 3995–4000 (2002).
[17]X. Hu, D. G. Cahill, and R. S. Averback, J. Appl. Phys. **93**, 165–169 (2003).
[18]F. Ruffino, R. De Bastiani, M. G. Grimaldi, C. Bongiorno, F. Giannazzo, F. Roccaforte, C. Spinella, and V. Raineri, Nucl. Instrum. Methods Phys. Res. B **257**, 810–814 (2007).
[19]A. Klimmer and P. Ziemann, Phys. Rev. B **79**, 155427 (2009).
[20]X. Meng, T. Shibayama, R. Yu, S. Takayanagi, and S. Watanabe, J. Mater. Sci. **48**, 920–928 (2013).
[21]L. Repetto, B. Setina Batic, G. Firpo, E. Piano, and U. Valbusa, Appl. Phys. Lett. **100**, 223113 (2012).
[22]X. Meng, T. Shibayama, R. Yu, S. Takayanagi, and S. Watanabe, Nucl. Instrum. Methods Phys. Res. B **314**, 112–116 (2013).
[23]X. Meng, T. Shibayama, R. Yu, S. Takayanagi, and S. Watanabe, J. Appl. Phys. **114**, 054308 (2013).
[24]S. J. Henley, J. D. Carey, and S. R. P. Silva, Phys. Rev. B **72**, 195408 (2005).
[25]C. Favazza, R. Kalyanaraman, and R. Sureshkumar, Nanotechnology **17**, 4229–4234 (2006).
[26]Y. Kojima and T. Kato, Nanotechnology **19**, 255605 (2008).
[27]A. E. Siegman and P. M. Fauchet, IEEE J. Quantum Electron. **22**, 1384–1403 (1986).
[28]A. Kiesow, S. Strohkark, K. Loschner, and A. Heilmann, Appl. Phys. Lett. **86**, 153111 (2005).
[29]S. Watanabe, Y. Yoshida, S. Kayashima, S. Yatsu, M. Kawai, and T. Kato, J. Appl. Phys. **108**, 103510 (2010).
[30]Y. Yoshida, S. Watanabe, Y. Nishijima, K. Ueno, H. Misawa, and T. Kato, Nanotechnology **22**, 375607 (2011).
[31]R. Yu, X. Meng, T. Shibayama, Y. Yoshida, S. Yatsu, S. Takayanagi, and S. Watanabe, Appl. Surf. Sci. **289**, 274–280 (2014).
[32]N. Kishimoto, N. Okubo, C. G. Lee, N. Umeda, and Y. Takeda, Nucl. Instrum. Methods Phys. Res. B **175–177**, 426–431 (2001).
[33]N. Kishimoto, N. Okubo, N. Umeda, and Y. Takeda, Nucl. Instrum. Methods Phys. Res. B **191**, 115–120 (2002).
[34]N. Okubo, N. Umeda, Y. Takeda, and N. Kishimoto, Nucl. Instrum. Methods Phys. Res. B **206**, 610–614 (2003).
[35]N. Kishimoto, N. Okubo, O. A. Plaksin, and Y. Takeda, J. Nucl. Mater. **329–333**, 1048–1052 (2004).
[36]N. Okubo, N. Kishimoto, and Y. Takeda, Nucl. Instrum. Methods Phys. Res. B **219–220**, 830–835 (2004).
[37]D. H. H. Hoffmann, A. Blazevic, P. Ni, O. Rosmej, M. Roth, N. A. Tahir, A. Tauschwitz, S. Udrea, D. Varentsov, K. Weyrich, and Y. Maron, Laser Part. Beams **23**, 47–53 (2005).
[38]Z. Yang, N. Sakaguchi, S. Watanabe, and M. Kawai, Sci. Rep. **1**, 190 (2011).
[39]Z. Yang, S. Watanabe, and T. Kato, Sci. Rep. **3**, 1201 (2013).
[40]J. F. Ziegler, J. P. Biersack, and U. Littmark, *The Stopping and Range of Ions in Solids* (Pergamon Press, New York, 1985).
[41]N. Sakaguchia, H. Kinoshitaa, S. Watanabea, Y. Sueishia, N. Akasakab, and H. Takahashi, J. Nucl. Mater. **382**, 197–202 (2008).
[42]C. Suryanarayana and T. R. Anantharaman, Mater. Sci. Eng. **13**, 73–81 (1974).
[43]W. F. Mc Clune, "Powder diffraction file: alphabetical index, inorganic phases," JCPDS-International Centre for Diffraction Data, Swarthmore, PA, Au: Card No. 4-0784, 1988.
[44]N. B. Dahotre and S. P. Harimkar, *Laser Fabrication and Machining of Materials* (Springer Science, New York, 2008), pp. 31–66.
[45]M. Quinten, *Optical Properties of Nanoparticle Systems: Mie and Beyond* (Wiley-VCH, Weinheim, 2011), pp. 277–278.
[46]See supplementary material at http://dx.doi.org/10.1063/1.4871016 for the change in spatial fluence profiles of the nanosecond-pulsed laser beam after transmission through a quartz glass window (S1); the nanoparticles are found to be a single crystal by the selected area electron diffraction pattern (S2); and grain size of an as-evaporated Au thin film on a $SiO_2$ glass substrate (S3).
[47]Y. Sasajima and K. Tanimura, Phys. Rev. B **68**, 014204 (2003).
[48]D. J. Srolovitz and S. A. Safran, J. Appl. Phys. **60**, 247–254 (1986).